CHIN. PHYS. LETT. Vol. 36, No. 9 (2019) 093701

Experimental Realization of Degenerate Fermi Gases of ^{87}Sr Atoms with 10 or Two Spin Components *

Wei Qi(祁卫)[1], Ming-Cheng Liang(梁明诚)[1], Han Zhang(张涵)[1], Yu-Dong Wei(魏玉栋)[1], Wen-Wei Wang(王文伟)[1], Xu-Jie Wang(王旭杰)[1], Xibo Zhang(张熙博)[1,2,3]**

[1]*International Center for Quantum Materials, School of Physics, Peking University, Beijing 100871*
[2]*Collaborative Innovation Center of Quantum Matter, Beijing 100871*
[3]*Beijing Academy of Quantum Information Sciences, Beijing 100193*

(Received 21 May 2019)

We report the experimental realization of quantum degenerate Fermi gases of ^{87}Sr atoms under controlled 10- and dual-nuclear-spin configurations. Based on laser cooling and evaporative cooling, we achieve an ultracold Fermi gas of 10^5 atoms equally distributed over 10 spin states, with a temperature of $T/T_F = 0.21$. We further prepare a dual-spin gas by optically pumping atoms to the $m_F = 9/2$ and $m_F = 7/2$ states and observe a slightly lower T/T_F than that for a 10-spin gas under the same trapping condition, showing efficient evaporative cooling under a decreasing number $\mathcal{N}$ of spin states ($\mathcal{N} \geqslant 2$) despite the increasing importance of Pauli exclusion. Given that rethermalization becomes less efficient with $\mathcal{N}$ approaching unity, we evaporatively cool an almost polarized gas to 130 nK. The simple and efficient preparation of ultracold Fermi gases of ^{87}Sr with tunable spin configurations provides a first step towards engineering topological quantum systems.

PACS: 37.10.De, 67.85.Lm, 67.85.−d DOI: 10.1088/0256-307X/36/9/093701

Experiments of alkaline-earth atoms have pushed the frontiers of fundamental physics.[1] In particular, experiments based on the fermionic strontium isotope (^{87}Sr), with up to $\mathcal{N} = 10$ nuclear spin states in ^{87}Sr and SU($\mathcal{N}$)-symmetric interatomic interactions hold promise for providing next-generation frequency standards,[2–4] exploring orbital magnetism,[5] studying many-body correlations[6,7] and topological physics,[8] simulating high-energy gauge-field physics such as lattice quantum chromodynamics (QCD),[9] improving quantum non-demolition measurements[10] and quantum metrology,[11] and producing highly coherent samples that are well controlled in all degrees of freedom.[12]

To enhance coherence in the external degrees of freedom, it is necessary to cool ^{87}Sr atoms into a quantum degenerate Fermi gas.[13–15] A degenerate Fermi gas not only enables researchers to explore the ground-state phase diagram and dynamics of a quantum system, but also enhances interatomic interactions.[16] Reaching low T/T_F is required for studying fermionic superfluidity,[17] algorithmic cooling,[18] and Fermi–Hubbard systems in optical lattices.[19] Furthermore, controlling the spin configuration of a degenerate gas is required for realizing some exotic topological orders. For example, to study the minimum model for a quantum anomalous Hall system, one needs to produce a dual-spin degenerate gas[20] or a spin-polarized gas.[21] So far, ^{87}Sr degenerate Fermi gases with $\mathcal{N} = 1$, 2, and 10 spins have been demonstrated,[22] although studies on quantitative control of atomic distribution over spin states remain sparse.

Here, we experimentally realize degenerate Fermi gases of ^{87}Sr under tunable spin configurations. First, we realize an almost equal statistical mixture of 10 nuclear spin states and evaporatively cool the gas to a lowest temperature of 34 nK and a lowest $T/T_F = 0.21^{+0.10}_{-0.04}$. Second, we optically pump atoms into a near-equal distribution over two spins ($m_F = 9/2$ and $7/2$), and observe a slightly lower T/T_F than that for a 10-spin gas under the same trapping condition, showing efficient evaporative cooling despite the enhanced role of the Pauli exclusion at a decreased number of spins. Lastly, we evaporatively cool an almost polarized sample (80% in the $m_F = 9/2$ state) to 130 nK, which is considered to be cold enough for our future optical lattice experiment.

Our ultracold strontium experiment focuses on fermionic ^{87}Sr and starts with laser cooling and trapping. Figure 1(a) shows the energy levels of strontium. A broad $^1S_0$–$^1P_1$ 461 nm transition underlies the transverse cooling, Zeeman slowing, and a first-stage magneto-optical trap (blue MOT). The narrow $^1S_0$–$^3P_1$ 689 nm transition allows for a second-stage magneto-optical trap (red MOT). Our new apparatus (Fig. 1(b)) centers on an ultrahigh vacuum (UHV) chamber made of titanium, where the pressure remains below 1×10^{-11} Torr during experimental op-

*Supported by the National Key Research and Development Program of China under Grant Nos 2016YFA0300901 and 2018YFA0305601, the National Natural Science Foundation of China under Grant No 11874073, and the International Center for Quantum Materials of Peking University.

**Corresponding author. Email: xibo@pku.edu.cn

© 2019 Chinese Physical Society and IOP Publishing Ltd

erations. To achieve this low pressure, we implement three special vacuum designs. First, the UHV chamber connects to vacuum pumps through large-inner-diameter tubes that provide hundreds of L/s vacuum conductance. Second, we install two complementary pumps: a 150 L/s ion pump (Gamma Vacuum) and a 1000 L/s getter pump (SAES, CapaciTorr D 1000). Lastly, we abandon the heated window in the Zeeman slowing path and instead place a room-temperature 45° dielectric mirror (Edmund Optics 64–447) in the UHV region.

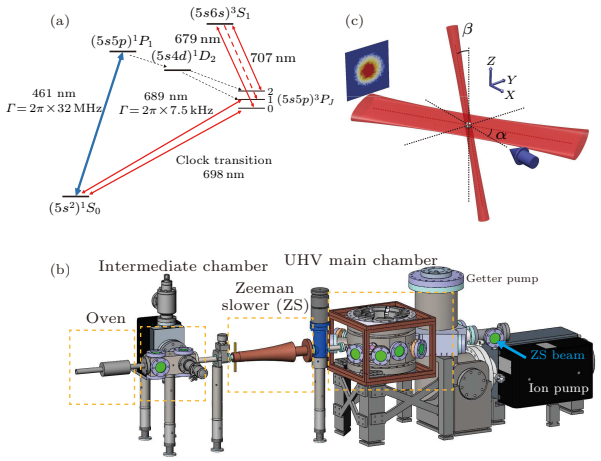

Fig. 1. Energy levels and experimental apparatus. (a) Relevant energy level diagram for the laser cooling and trapping of ^{87}Sr. (b) The UHV system. From left to right are the oven, intermediate chamber, Zeeman slower (ZS), and UHV main chamber. (c) A schematic diagram for the crossed dipole trap and absorption imaging. The horizontal dipole beam is at an angle of $\alpha \approx 30°$ with respect to the X axis that is also the imaging direction; the vertical beam propagates upwards at $\beta \approx 25°$ with respect to the Z axis (vertical direction).

To address the $^1S_0$–$^1P_1$ transition with 32 MHz linewidth, we lock the frequency of a 461 nm 'master' diode laser with sub-MHz instability to a strontium hollow-cathode lamp (Hamamatsu Photonics L2783-38NE-SR) using frequency modulation spectroscopy. This master laser injection-locks three slave lasers, each with about 100 mW power. Because atoms at the $^1P_1$ state have a small probability to leak into the long-lived $^3P_2$ state,[23] we build two 'repumper' lasers that operate at 679 nm and 707 nm (Fig. 1(a)) to ensure that atoms return to the $^1S_0$ ground state. The 707 nm laser frequency is modulated at 1 kHz frequency in a 5 GHz range, while the 679 nm laser frequency is locked to a commercial wavelength meter. Our experiment starts with thermal atoms emitted from a 560℃ oven. We perform two-dimensional transverse cooling to reduce the atomic beam divergence, and we then apply longitudinal Zeeman slowing to decelerate atoms before they are captured by the blue MOT. Transverse cooling and Zeeman slowing typically enhance the MOT atom number by factors of 2 and 25, respectively. We trap 4×10^7 ^{87}Sr atoms at several-millikelvin temperatures in the blue MOT.

To address the $^1S_0$–$^3P_1$ transition with 7.5 kHz linewidth, we phase-lock a commercial 689 nm red master laser (Toptica DL pro) to a high-finesse ($\mathcal{F} \approx 2 \times 10^5$) optical cavity using the Pound–Drever–Hall (PDH) approach. To take into account the hyperfine splittings of the $^3P_1$ level of ^{87}Sr, we in turn use the red master to injection-lock two slave lasers: a trapping laser operating on $^1S_0$ $(F = 9/2)$–$^3P_1$ $(F' = 11/2)$ to achieve cooling and trapping, and a stirring laser operating on $^1S_0$ $(F = 9/2)$–$^3P_1$ $(F' = 9/2)$ to redistribute atoms in the $^1S_0$ nuclear spin sublevels. To efficiently transfer atoms from the blue MOT at millikelvin temperatures to the red MOT, we modulate both the trapping and stirring laser frequencies by about 6 MHz for 300 ms, and then turn off both frequency modulations for cooling to lower temperatures. We trap 1.2×10^7 atoms at 4 μK temperature after 470 ms of red MOT loading. Without optical pumping, these atoms distribute almost equally over 10 nuclear spin states.[7]

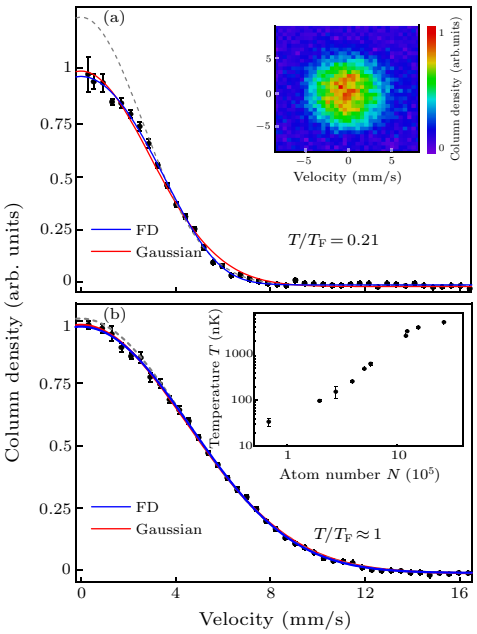

Fig. 2. Evaporatively cooled 10-spin Fermi gases. (a) Azimuthally averaged velocity distribution for a degenerate Fermi gas: data (solid circles), a global Maxwell–Boltzmann fit (red line), a global Fermi–Dirac fit (blue line), and a Maxwell–Boltzmann fit to the low-density tail (gray dashed line) using data outside the disk of radius $\sqrt{2}\rho$, where ρ is the rms radius of the cloud, while both Maxwell–Boltzmann fits deviate from the data, the Fermi–Dirac fit accurately describes the data with a fitted $T/T_F = 0.21^{+0.10}_{-0.04}$. The inset shows the two-dimensional velocity distribution obtained by performing absorption imaging after a 27 ms time-of-flight (TOF) and averaged over five experimental repetitions. (b) Velocity distribution for a gas at a higher $T/T_F \approx 1$, where all three fits are close to each other. Inset: temperature as a function of atom number, showing a trace of evaporative cooling. Uncertainties represent the 1σ statistical standard errors.

To perform evaporative cooling, we next load atoms into a crossed dipole trap (Fig. 1(c)). Two 1064 nm beams are generated by a commercial laser (Coherent Mephisto MOPA42) and delivered to the main chamber by two high-power optical fibers (OZ Optics). As Fig. 1(c) shows, an elliptical beam along the horizontal direction has horizontal and vertical $1/e^2$ radii of 230 μm and 30 μm, respectively. A circular beam along the near-vertical direction has a $1/e^2$ radius of 47 μm. Initially, we use a typical power of 7 W for the horizontal beam and 6.5 W for the vertical beam. About 2×10^6 atoms are loaded into the dipole trap from the red MOT, held for 500 ms of plain evaporation, and then cooled into quantum degeneracy based on 9.5 s of forced evaporation. Figures 2(a) and 2(b) show the data for azimuthally averaged velocity distribution obtained via blue-laser absorption imaging after 27 ms of time of flight (TOF) for a quantum degenerate Fermi gas and a near-thermal gas, respectively. These data are fitted using Maxwell–Boltzmann and Fermi–Dirac velocity distributions. We observe different features in Figs. 2(a) and 2(b). For a quantum degenerate gas (Fig. 2(a)), a global Maxwell–Boltzmann fit shows small but discernible deviation from the data, while a local Maxwell–Boltzmann fit to the low-density tail significantly overestimates the center density when extrapolated to small velocities. Therefore, we need the Fermi–Dirac expression[13,24] to fit the data correctly,

$$f(v_Y, v_Z) = -\frac{m(k_B T)^2}{2\pi(h\bar{f})^3}\mathrm{Li}_2[-\xi e^{-(m(v_Y^2+v_Z^2)/2k_B T)}],$$

where $v_{Y,Z}$ are the velocity components, Li_n is a polylogarithmic function of order n, and ξ is the fugacity. We determine T/T_F using the relation $\mathrm{Li}_3[-\xi] = -1/[6(T/T_F)^3]$. The Fermi–Dirac fit in Fig. 2(a) gives $T/T_F = 0.21^{+0.10}_{-0.04}$, which indicates quantum degeneracy. By contrast, for a near-thermal gas (Fig. 2(b)), there is negligible difference between the fitted Maxwell–Boltzmann and Fermi–Dirac velocity distributions. Because the Fermi–Dirac fitting has a large uncertainty of T/T_F at relatively high temperatures,[13,24] we determine $T/T_F \approx 1$ for Fig. 2(b) based on an alternative method that determines T and T_F individually. Here, the temperature T is measured by performing TOF, while the Fermi temperature $T_F = (6N/M)^{1/3}h\bar{f}/k_B$ is determined by the geometric mean $\bar{f}$ of measured trap frequencies in three spatial directions, the total atom number N, and the number of spin states M. The inset of Fig. 2(b) shows that by losing slightly more than a factor of 10 in atom number, we lower the temperature by two orders of magnitude down to 34 nK.

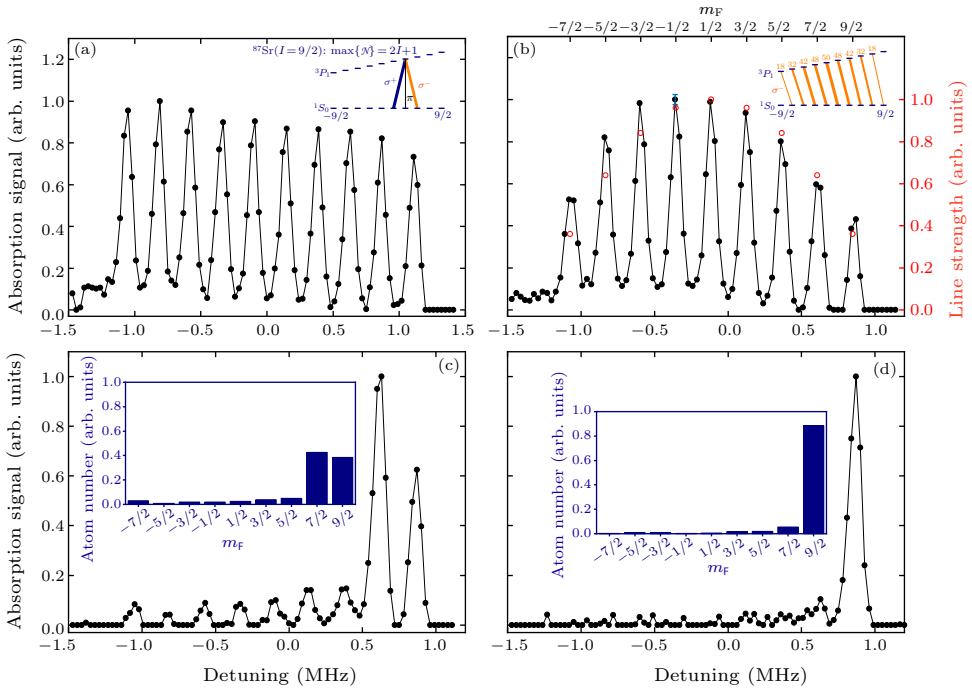

Fig. 3. Detecting and manipulating the atomic distribution over 10 nuclear spin states. Atomic signals are extracted from the 689 nm (red) absorption images taken at a bias field of 3 G. [(a), (b)] Detecting the atomic distributions. Here, the imaging beam has a linear polarization at the 'magic angle' (a) and a σ^- circular polarization (b), respectively. The inset in (a) shows the relevant transitions. The inset in (b) shows the relative strengths of the nine σ^- transitions. Red circles in (b) are the line strengths computed for an ideal σ^- imaging beam. [(c), (d)] Manipulating the atomic distributions. Here absorption signals are obtained using an imaging beam of σ^- polarization after optically pumping the atoms to a near-dual-spin configuration and to an almost spin-polarized configuration. The insets in (c) and (d) show the number percentage of atoms distributed over the spin states.

To verify how atoms populate in ground-state nuclear spin sublevels before evaporation, we use the same narrow-line transition as that used by the stirring laser to perform 689 nm (red) absorption imaging at a bias field of 3 G. This bias field splits the $^1S_0$ $(F = 9/2)$–$^3P_1$ $(F' = 9/2)$ transition into a group of transition lines with a uniform spacing of about 260 kHz. We first image atoms that are almost equally distributed over 10 spin states. For Fig. 3(a), we use an imaging beam of linear polarization at about 55° to the quantization axis (the Z axis), which is close to the 'magic angle' of 54.6° that gives the same atom-photon scattering cross section for each spin state,[25] and observe near-equal transition strengths. For Fig. 3(b), we use an imaging beam of σ^- polarization with respect to a different quantization axis along X. Here only nine transitions are allowed and the measured transition strengths agree fairly well with computed values. The small discrepancy is related to technical factors, such as imperfect circular polarization. We further prepare partially spin-polarized samples for future studies. Figures 3(c) and 3(d) show the atomic distributions obtained by optically pumping the atoms using a frequency-modulated red beam of σ^+ polarization and then imaging them with the σ^--polarized beam. We control the final spin configuration by varying the center frequency and frequency-modulation range of the optical pumping beam. The insets in Figs. 3(c) and 3(d) show the number percentage of atoms distributed over spin states, which are determined via normalizing the absorption signals by the measured transition strengths (shown in Fig. 3(b)). In Fig. 3(c), the population ratio between the $m_F = 7/2$ state (42% of the atoms) and $m_F = 9/2$ state (39% of the atoms) is approximately 1:1. In Fig. 3(d), about 89% of the atoms populate in the $m_F = 9/2$ state.

A bias field needs to be applied to maintain the atomic spin distribution during evaporation.[22] Figure 4 shows the measurements on spin-changing processes under different bias fields. Here we initially pump most atoms into the $m_F = 9/2$ state, ramp the bias field from 3 G to different values, hold atoms for 5 s in the dipole trap, and finally ramp the bias field back to 3 G before performing red absorption imaging. When we reduce the bias field to 0.08 G or lower values during the holding period, the gas shows significant depolarization. We conclude that a finite bias field is needed to prevent the above-mentioned spin-changing processes, and thus apply 0.7 G during the actual evaporative cooling. We experimentally confirm that, if the system is initially prepared in a multiple-spin configuration and held under a 0.7 G field, the atom number distribution will remain the same.

We find no significant increase of the final temperature when performing evaporation using two spin states as compared with the case using 10 states. In fact, we achieve $T/T_F = 0.24^{+0.04}_{-0.04}$ for a dual-spin configuration and $T/T_F = 0.28^{+0.05}_{-0.04}$ for a 10-spin case under the same trapping condition. The slightly lower T/T_F observed for the dual-spin configuration shows that the evaporative cooling efficiency remains sufficiently high under the decreasing number $\mathcal{N}$ of spin states ($\mathcal{N} \geq 2$) despite the increasing importance of Pauli exclusion, while rethermalization becomes less efficient as $\mathcal{N}$ approaches unity, we evaporatively cool an almost polarized sample (with about 80% of the atoms populated in the $m_F = 9/2$ state and about 20% in the other states) to 130 nK, which corresponds to an energy scale lower than other typical energy scales in our future optical lattice experiment and is thus considered to be cold enough.

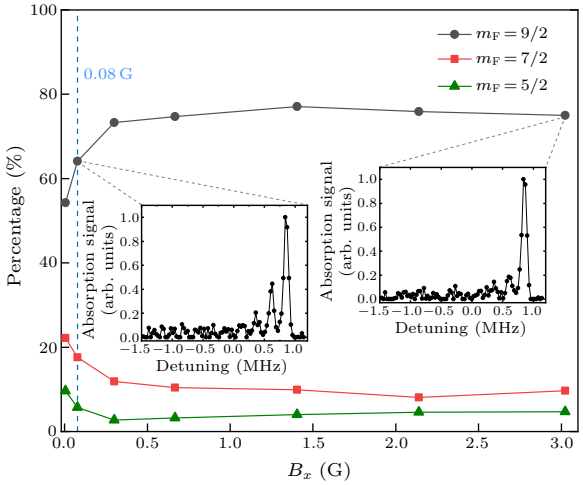

Fig. 4. Spin-changing processes in the crossed dipole trap under different bias fields. Atoms are initially prepared in an almost polarized spin configuration (right-hand inset) under a 3 G bias field, and then held under various field values ($B = |B_x|$, $B_y = B_z = 0$) for 5 s. The final number percentages of three spin states are shown: 9/2 (circles), 7/2 (squares), 5/2 (up triangles).

In conclusion, we have evaporatively cooled ^{87}Sr atoms into degenerate Fermi gases with $T/T_F \approx 0.2$ under controlled 10- and dual-spin configurations. Our efficient cooling and spin manipulation for ^{87}Sr provide a starting point for engineering and probing correlated topological quantum gases, such as the minimum model for a quantum anomalous Hall system.[20] In addition, our lowest T/T_F may be currently limited by dipole beam intensity noise or reduced collision rates due to the decreased trap frequencies at the end of evaporation. Deeper Fermi degeneracy can be pursued by applying more stable control of dipole beam intensities and by implementing a tighter dipole confinement along the gravity direction to ensure effective rethermalization at very low trap depths.

We are grateful to Ze-Feng Ren, Qian Wang, Wei-

Xuan Guo, Tian-Xing Zheng, Ze-Yang Li, Qi-Zhi Li, Xue-Yang Han, Si-Wei Zhang, Yao-Yuan Fan, Tong Wang for assistance and technical support during the apparatus construction.

References

[1] Daley A J, Boyd M M, Ye J and Zoller P 2008 *Phys. Rev. Lett.* **101** 170504
[2] Campbell S L, Hutson R B, Marti G E, Goban A, Oppong N D, McNally R L, Sonderhouse L, Robinson J M, Zhang W, Bloom B J and Ye J 2017 *Science* **358** 90
[3] Lin Y G , Wang Q, Li Y, Meng F, Lin B K , Zang E J , Sun Z, Fang F, Li T C and Fang Z J 2015 *Chin. Phys. Lett.* **32** 090601
[4] Tian X, Xu Q, Yin M, Kong D, Wang Y, Lu B, Liu H, Ren J and Chang H 2015 *Acta Opt. Sin.* **35** s102001
[5] Tokura Y and Nagaosa N 2000 *Science* **288** 462
[6] Martin M J, Bishof M, Swallows M D, Zhang X, Benko C, von-Stecher J, Gorshkov A V, Rey A M and Ye J 2013 *Science* **341** 632
[7] Zhang X, Bishof M, Bromley S L, Kraus C V, Safronova M S, Zoller P, Rey A M and Ye J 2014 *Science* **345** 1467
[8] Kolkowitz S, Bromley S L, Bothwell T, Wall M L, Marti G E, Koller A P, Zhang X, Rey A M and Ye J 2017 *Nature* **542** 66
[9] Banerjee D, Bögli M, Dalmonte M, Rico E, Stebler P, Wiese U J and Zoller P 2013 *Phys. Rev. Lett.* **110** 125303
[10] Eckert K, Romero-Isart O, Rodriguez M, Lewenstein M, Polzik E S and Sanpera A 2008 *Nat. Phys.* **4** 50
[11] Ludlow A D, Boyd M M, Ye J, Peik E and Schmidt P O 2015 *Rev. Mod. Phys.* **87** 637
[12] Zhang X and Ye J 2016 *Natl. Sci. Rev.* **3** 189
[13] DeSalvo B J, Yan M, Mickelson P G, Martinez de E Y N and Killian T C 2010 *Phys. Rev. Lett.* **105** 030402
[14] Tey M K, Stellmer S, Grimm R and Schreck F 2010 *Phys. Rev. A* **82** 011608
[15] Stellmer S, Schreck F and Killian T C 2014 *Annu. Rev. Cold Atoms Molecules* vol 2 chapter 1 p 1
[16] Goban A, Hutson R B, Marti G E, Campbell S L, Perlin M A, Julienne P S, D'Incao J P, Rey A M and Ye J 2018 *Nature* **563** 369
[17] Ku M J H, Sommer A T, Cheuk L W and Zwierlein M W 2012 *Science* **335** 563
[18] Bakr W S, Preiss P M, Tai M E, Ma R, Simon J and Greiner M 2011 *Nature* **480** 500
[19] Esslinger T 2010 *Annu. Rev. Condens. Matter Phys.* **1** 129
[20] Liu X J , Law K T and Ng T K 2014 *Phys. Rev. Lett.* **112** 086401
[21] Zhang L, Zhang L and Liu X J 2019 *Phys. Rev. A* **99** 053606
[22] Stellmer S, Grimm R and Schreck F 2011 *Phys. Rev. A* **84** 043611
[23] Yasuda M and Katori H 2004 *Phys. Rev. Lett.* **92** 153004
[24] DeMarco B 2001 *PhD Dissertation* (University of Colorado at Boulder)
[25] Campbell S L 2017 *PhD Dissertation* (University of Colorado at Boulder)